ELSEVIER

NeuroImage

www.elsevier.com/locate/ynimg
NeuroImage 39 (2008) 1706–1720

Localization of correlated network activity at the cortical level with MEG

Jan Kujala,[a,*] Joachim Gross,[b] and Riitta Salmelin[a]

[a]*Brain Research Unit, Low Temperature Laboratory, Helsinki University of Technology, PO Box 5100, FIN-02015 TKK, Espoo, Finland*
[b]*Centre for Cognitive Neuroimaging, Department of Psychology, University of Glasgow, UK*

Received 6 June 2007; revised 23 October 2007; accepted 24 October 2007
Available online 12 November 2007

In both hemodynamic and neurophysiological imaging methods, analysis of functionally interconnected networks has typically focused on brain areas that show strong activation in specific tasks. Alternatively, connectivity measures may be used directly to localize network nodes, independent of their level of activation. This approach requires initial cortical reference areas which may be identified based on their high level of activation, their coherence with an external reference signal, or their strong connectivity with other brain areas. Irrespective of how the nodes have been localized the mathematical complexity of the analysis methods precludes verification of the accuracy and completeness of the network structure by direct comparison with the measured data. Therefore, it is critical to understand how the choices of parameters and procedures used in the analysis affect the network identification. Here, using simulated and measured magnetoencephalography (MEG) data, and Dynamic Imaging of Coherent Sources (DICS) for connectivity analysis, we quantify the veracity of network detection at the individual and group level as a function of relevant parameter choices. Using simulations, we demonstrate that coupling measures enable accurate identification of the network structure even without external reference signals, and illustrate the applicability of this approach to real data. We show that a valid estimate of interindividual variability is critical for reliable group-level analysis. Although this study focuses on application of DICS to MEG data, many issues considered here, especially those regarding individual vs. group-level analysis, are likely to be relevant for other neuroimaging methods and analysis approaches as well.
© 2007 Elsevier Inc. All rights reserved.

Introduction

Evidence from intracranial recordings suggests that areas forming cerebral networks connect via synchronized neuronal firing (Singer, 1999; Tallon-Baudry et al., 2001). Positron emission tomography (PET) and functional magnetic resonance imaging (fMRI) studies have assessed functional and/or effective connectivity between brain areas (Büchel and Friston, 1998; Mechelli et al., 2002; Penny et al., 2004; Mechelli et al., 2005). In hemodynamic connectivity analyses, the potential network nodes are usually preselected among areas that are more active in a specific task than in a control condition, and the models describing the interactions are constructed based on *a priori* hypotheses of cortical integration (Büchel and Friston, 1997; Friston et al., 2003). In data-driven analysis approaches one would like to find the functionally coupled brain areas directly using connectivity measures, without *a priori* assumptions based on the overall level of activation. A neural population may exhibit an equal amount of activity in different conditions and, thus, not be revealed in contrast analysis, although its coupling with other areas could vary between conditions. Estimation of directed causality between brain areas (Granger causality; Roebroeck et al., 2005) may provide a means for identification of network nodes directly from the fMRI signals, without prior selection of network nodes based on the level of activation.

Magnetoencephalography (MEG) and electroencephalography (EEG) allow real-time tracking of synchronously firing neural populations. While intuitively they are optimally suited for direct detection and characterization of functional coupling, the equivocal relationship between electromagnetic fields and neuronal sources has limited coherence analysis mostly to the sensor level, without extending to the actual brain areas (Gerloff et al., 1998; Sarnthein et al., 1998; Andres et al., 1999; Rodriguez et al., 1999; von Stein et al., 1999; Gross et al., 2004; Palva et al., 2005). Similarly to the typical approach in exploring hemodynamic connectivity, some EEG and MEG studies have constructed networks at cortical level based on the overall level of activation (Cosmelli et al., 2004; Astolfi et al., 2005) or difference in rhythmic power between experimental conditions (Gross et al., 2004) and estimated interaction between those areas.

Only a handful of studies have sought to directly localize interacting cortical areas based on correlation measures (Gross et al., 2001; Gross et al., 2002; Schnitzler and Gross, 2005; Jerbi et al., 2007). Many of those MEG studies employed Dynamic Imaging of Coherent Sources (DICS), in which a frequency-domain spatial filter is used to estimate time-courses of neural activity in different cortical areas and coupling between areas

* Corresponding author. Fax: +358 9 451 2969.
E-mail address: jjkujala@neuro.hut.fi (J. Kujala).
Available online on ScienceDirect (www.sciencedirect.com).

1053-8119/$ - see front matter © 2007 Elsevier Inc. All rights reserved.
doi:10.1016/j.neuroimage.2007.10.042

(Gross et al., 2001). As these experiments focused on the motor system, electromyogram (EMG) recorded from the moving arm/hand muscles served as an external reference signal. The EMG–MEG coherence allowed localization of the primary motor cortex which, in turn, provided a cortical reference area for detection of other functionally coupled brain areas. In realistic cognitive tasks, meaningful nonbrain reference signals are usually not available and, therefore, network structure must be determined directly from brain activity. Recently, with further development of the DICS method, we identified and characterized a left-hemisphere network in continuous reading (Kujala et al., 2007).

When seeking answers to neuroscience questions, estimation of interactions between cortical areas can be problematic. Regardless of whether one uses hemodynamic or neurophysiological imaging methods, it is impossible to directly verify from the originally recorded signals whether the results of the analysis give a complete picture of connectivity, e.g., by estimating whether the identified areas fully explain the variance in the data. Thus, in order to utilize connectivity analysis in a manner that accurately describes cerebral interactions, it is essential to understand the effects of critical parameters and specific choices that need to be made at different stages of the analysis. Here, we used both simulated and measured MEG data to quantify such effects on individual and group-level results in the data-driven DICS analysis procedure. The present evaluation includes the following steps: (1) estimation of frequency ranges of interest; (2) identification of cortical reference area(s); (3) cortico-cortical mapping; (4) significance estimation for coherent connections; (5) network identification at group level. In real data, network nodes may not be detectable by their level of activity but only with the help of connectivity measures (Gross et al., 2002; Kujala et al., 2007). The present simulations were constructed for the most general case in which connectivity analysis is required for network identification. The data set was designed to resemble real data, including multiple subjects with interindividual variability in the location of functional areas and complete with noise and background activity, thus facilitating controlled investigation of parameter values and choices made at different stages of analysis that provide insights into network analysis of real neuroimaging data. In localization of network nodes, we use coherence as the measure of connectivity (Gross et al., 2001). Linearity makes the calculation computationally feasible but, obviously, this type of analysis may fail to reveal areas whose interactions are nonlinear.

The accuracy of localizing network nodes was compared when the search was initiated from an external reference signal or when it was based on connection density estimation (CDE). We evaluated the influence of grid size (which defines the spatial sampling), regularization (which determines the spatial extent of source representation), and required minimum distance between candidate nodes (which affects the amount of spurious coupling due to leakage between spatial filters) on the sensitivity and accuracy of the network identification. Detection of network nodes from individual vs. group-level maps was evaluated both at the stage of selecting reference areas and at the subsequent stage of cortico-cortical search. Furthermore, at both stages, simulated data were used to test the effect of interindividual variability on the localization of the corresponding nodes. These analyses were aimed at obtaining estimates of the extent to which the increased statistical power of group-level analysis outweighs the interindividual variability in the localization of interacting areas and, thus, whether group-level analysis can be recommended for the amount of spatial variability observed in real data. The concepts emerging from the simulation study are demonstrated on two real data sets, a motor task with muscle activity as an external reference signal and a reading task in which direct cortico-cortical connectivity analysis is the only plausible option. Although this study focuses on the application of DICS to MEG data for extracting networks of functionally coupled brain areas, many of these considerations are conceptually relevant for all analysis methods that are used to image and estimate neural connectivity based on neurophysiological or hemodynamic data.

Methods

Dynamic imaging of coherent sources (DICS)

DICS (Gross et al., 2001) is a beamforming technique (Sekihara and Scholz, 1996; Robinson and Vrba, 1997; Van Veen et al., 1997; Gross and Ioannides, 1999; Hillebrand et al., 2005) in which the oscillatory components and their linear interactions are represented as a cross-spectral density matrix ($N\times N\times F$; N=number of MEG sensors, F=number of frequency bins). From the cross-spectral density matrix, it is possible to derive two measures, power and coherence. Coherence is obtained by normalizing the cross-spectral density between two signals with their power spectral densities. In DICS, a linear transformation (based on a constrained optimization problem), which acts as a spatial filter, is used to image power and coherence in the brain at a given frequency range. The transformation is attained by minimizing the variance of the output of the spatial filter while constraining the filter such that activity of the source at position r is passed with unit gain:

$$\min[E\{||\mathbf{A}M||^2\} + \alpha||\mathbf{A}||] \text{ subject to } \mathbf{AL}(\mathbf{r}) = \mathbf{I}, \quad (1)$$

where E is the expectation value, $\mathbf{A}$ the linear transformation matrix (spatial filter), M the Fourier transformed data, $\mathbf{I}$ the unit matrix, and α the regularization parameter. The columns of $\mathbf{L}(\mathbf{r})$ contain the solution of the forward problem for two orthogonal tangential unit dipoles at $\mathbf{r}$. In a spherical conductor, such dipoles span the space containing all possible source orientations that can be detected with MEG. In the Results, we express the regularization parameter relative to the largest eigenvalue of $\mathbf{C}(f)$, where $\mathbf{C}(f)$ is the cross spectral density at a specific frequency bin or range, i.e., $\alpha=\lambda_{\max}\alpha_{\text{rel}}$, where $\lambda_{\max}$ is the largest eigenvalue and α_{rel} is the relative regularization. The frequency-dependent solution of Eq. (1) is

$$\mathbf{A}(\mathbf{r},f) = (\mathbf{L}^T(\mathbf{r})\mathbf{C}_\mathbf{r}(f)^{-1}\mathbf{L}(\mathbf{r}))^{-1}\mathbf{L}^T(\mathbf{r})\mathbf{C}_\mathbf{r}(f)^{-1}, \quad (2)$$

where $\mathbf{C}_\mathbf{r}(f)=\mathbf{C}(f)+\alpha\mathbf{I}$. The cross spectrum between the tangential source combinations at the two locations ($\mathbf{r_1}$, $\mathbf{r_2}$) can then be estimated as

$$\mathbf{C_s}(\mathbf{r_1},\mathbf{r_2},f) = \mathbf{A}(\mathbf{r}_1,f)\mathbf{C}(f)\mathbf{A}^{*T}(\mathbf{r}_2,f). \quad (3)$$

In the special case when $\mathbf{r_1}$ equals $\mathbf{r_2}$, $\mathbf{C_s}$ represents the estimate of signal power at each location. If the singular values of $\mathbf{C_s}$ fulfill $\lambda_1 >> \lambda_2$ the cross spectrum, and thus both coherence and power estimates can be attributed to sources with fixed orientations. If the singular value relation does not hold, power and coherence estimates can be obtained by using the trace of the matrix $\mathbf{C_s}(\mathbf{r_1},\mathbf{r_2},f)$. The singular value relation also provides an alternative approach in which the coherence estimation may be limited to sources which have a fixed orientation. This assumption is well

grounded in neurophysiology as detection of neuronal events with MEG requires simultaneous activation of thousands of pyramidal cells in a small cortical patch, with the parallel orientation of their apical dendrites allowing summation of the neural currents. Sources with a salient, dominant direction of current flow are thus more likely to represent accurate localization of a focal functional area than sources with no preferred (random) direction.

The dense sensor spacing of the whole-head MEG systems used in the present study samples the signals from the entire brain without spatial aliasing (Ahonen et al., 1993), and with beamforming techniques, one can obtain an estimate of the signals originating from any given location in the brain (Van Veen et al., 1997). As the accuracy of MEG is around 2–3 mm under favorable conditions (Hämäläinen et al., 1993), the beamformer estimation is typically performed with a grid spacing of some millimeters, covering the entire brain. The DICS tomographic maps are formed by calculating the power and coherence estimates at all grid points and overlaying them on individual anatomical magnetic resonance images (MRI). The reference signal used in coherence calculation can be either an external signal or the beamformer estimate of activity originating from a selected cortical location. Power maps are presented as power statistical maps (pSPM) and the 99% confidence level for coherence can be estimated using surrogate data (Priestley, 1981). Once brain areas are identified, their time-courses can be extracted using the spatial filter (Van Veen et al., 1997).

Selection of frequency range

With DICS a frequency range must be selected before the spatial filter is applied to the data. Frequencies at which there is high oscillatory power and modulation between conditions can be estimated by calculating the power spectra at sensor level. As the background rhythmic activity can mask small task-related effects and as frequencies at which there are task-related changes of oscillatory power may not coincide with those frequencies which subserve interaction between cortical areas, it is also important to evaluate connectivity as a function of frequency. This was done by counting for each MEG sensor the number of other sensors with which it showed significant coherence. The significance levels were estimated using surrogate data (Priestley, 1981). To focus on long-range coherence, the two nearest sensors in each direction were excluded from the coherence estimation.

Finding reference areas

In mapping cortico-cortical coherence, at least one suitable cortical reference area is required. We focused on two approaches, the use of external reference signals and connection density estimation (CDE). In CDE analysis, the brain was divided into voxels of varying side length (6–12 mm at 2-mm steps) and coherence was computed for all voxel combinations. CDEs were obtained by counting, for each voxel, the number of connections for which coherence exceeded a chosen threshold, beyond the immediate neighborhood of the voxel (distance 4, 5, or 6 cm). The effect of relative regularization that determines spatial specificity was tested for three levels (α_{rel}=0.01, 0.001, 0.0001). This initial search was limited to the cortex (max. 15 mm below the cortical surface) where the spatial resolution of MEG is best. For the measured data sets, the CDE analysis was performed within the left-hemisphere cortex. Because of the large number of connections to be evaluated (millions of connections at this grid size), it was not computationally feasible to estimate confidence levels (using surrogate data) for each connection. Therefore, a fixed level of coherence (0.1) was adopted at this stage, and confidence levels were evaluated only for the final set of connections. The CDE results were presented as normalized density statistical parametric maps (dSPM), overlaid on anatomical MRIs (Dale et al., 2000). Each point in these maps gives the relative amount of connections from that voxel to all other voxels in the brain. Focal maxima from these maps were taken as initial reference areas. When the experiment included multiple conditions, contrast connection density estimates (cCDE) were additionally computed by excluding connections for which coherence exceeded the threshold in both conditions.

Cortico-cortical mapping

Starting from the reference areas, DICS was used to compute coherence maps separately for each subject, with a 6-mm grid size. Local maxima in the maps were identified as candidate nodes. The confidence level of each connection was estimated using surrogate data (Priestley, 1981; Halliday et al., 1995; Faes et al., 2004; Patel et al., 2006). First, the time-courses of activation at the identified areas were reconstructed using the spatial filter. Surrogate data were then created by applying the same random permutation of data samples for the time-series at both ends of a connection. This type of surrogate data tests specifically for spurious coherence due to leakage between spatial filters. If the two time-series have common components due to the same activity seen at two sites (leakage between spatial filters), also the shuffled time-series show similar behavior. If, however, coherence results from two independent yet correlated time-series, the shuffling destroys the similarity between the time-series. Confidence levels for coherence were obtained by estimating coherence between the surrogate series and by computing the frequency histogram for coherence. Coherence threshold was set to the desired percentile (here 99%) of the coherence sampling distribution.

For evaluation of the networks at the group level, the individual coherence data, in form of distributed maps or discrete significant nodes, were transferred to a common coordinate system using an elastic transformation (Schormann and Zilles, 1998). The inter-subject consistency of the coherence maps was evaluated with a one-sample *t*-test in the SPM2 software (Wellcome Department of Imaging Neuroscience, University College London, UK, http://www.fil.ion.ucl.ac.uk/spm/spm2.html). For the significant nodal points, commonalities in the network structure were determined by giving the individual nodes a spatial extent to account for the spatial sampling resolution and individual variability in the functional location of the regions, and by setting the data value in each voxel within that extent to 1 or 0; 1 indicated that there was at least one significant connection to/from that area, and 0 that there was none. The intersubject consistency was tested using SPM2, and areas passing this test were taken as group-level nodal points of the network. The effect of spatial extent on network identification was tested by giving the individual nodes an extent of 1, 1.5, or 2 times the grid size. The effect of interindividual variability in the locations of functionally similar cortical areas (e.g., 9–13 mm in complex language tasks; Xiong et al., 2000) was tested by introducing into the node locations no variation or random variation of 1 or 2 times the grid size.

Comparison of localization results

A one-sample *t*-test was used to test whether a reference area was systematically mislocalized in any direction (*x*,*y*,*z*), and whether its location was influenced by the analysis approach (e.g., EMG–MEG coherence vs. CDE). Source locations determined at the individual vs. group level were compared using a paired samples *t*-test. ANOVAs were employed for testing the influence and interaction of multiple analysis parameters on source localization.

Constructing the simulation

Simulated data were constructed in such a way that the areas forming the cortico-cortical network could not be localized based on their oscillatory power but that localization of coherence was required for their identification. This is the most general (and most difficult) case, and it has been encountered in real data sets (Gross et al., 2002; Kujala et al., 2007). The data set, 4 min in duration, was composed of five interacting neural sources, two additional sources that were not functionally coupled with the other areas, and background noise (Fig. 1a). The neural sources were represented by current dipoles. The time-courses of activation in the source areas were created by setting instantaneous frequencies at each time-point and by then generating the corresponding frequency modulated signals. The instantaneous frequencies consisted of a base frequency and a random component. For the interacting sources, the base frequency was set to 15 Hz, and the random component for each source was set so that the instantaneous frequencies fell between 14 and 16 Hz at all time-points. The random components were varied until all the sources were coherent with each other (coherence between 0.2 and 0.6).

The two noncoherent sources were included in order to mask the oscillatory power of the coherent sources, while not interfering with their mutual coupling. The time-series of the noncoupled sources were generated by combining two different base frequencies for each source; 9 Hz (strong) and 24 Hz (weak) for source 1, and 10 Hz (weak) and 22 Hz (strong) for source 2. These sources were more powerful than the interacting sources, even around 15 Hz (Fig. 1c), thus effectively masking their activity.

Noise in the simulation was generated by combining white noise at sensor level and background activity at source level. This combination provides a more realistic noise profile than either cortical or sensor-level noise types alone. The "noise" sources representing background brain activity were simulated by placing sources at regular 2-cm intervals throughout the brain, excluding deep structures (approximately 150 sources per subject; Fig. 1a). Their time-series were created by band-pass filtering white noise to frequency ranges 5 Hz in width, with the maximum at a random frequency between 5 and 45 Hz. With the added noise the extractable coherencies between the interacting sources fell between 0.05 and 0.3. Fig. 1b shows the coherence between the 5 interacting areas with and without the added noise component.

In addition to the cortical signals, an independent signal which was coherent with the time-series of one neural source was generated to exemplify an external reference signal (e.g., EMG).

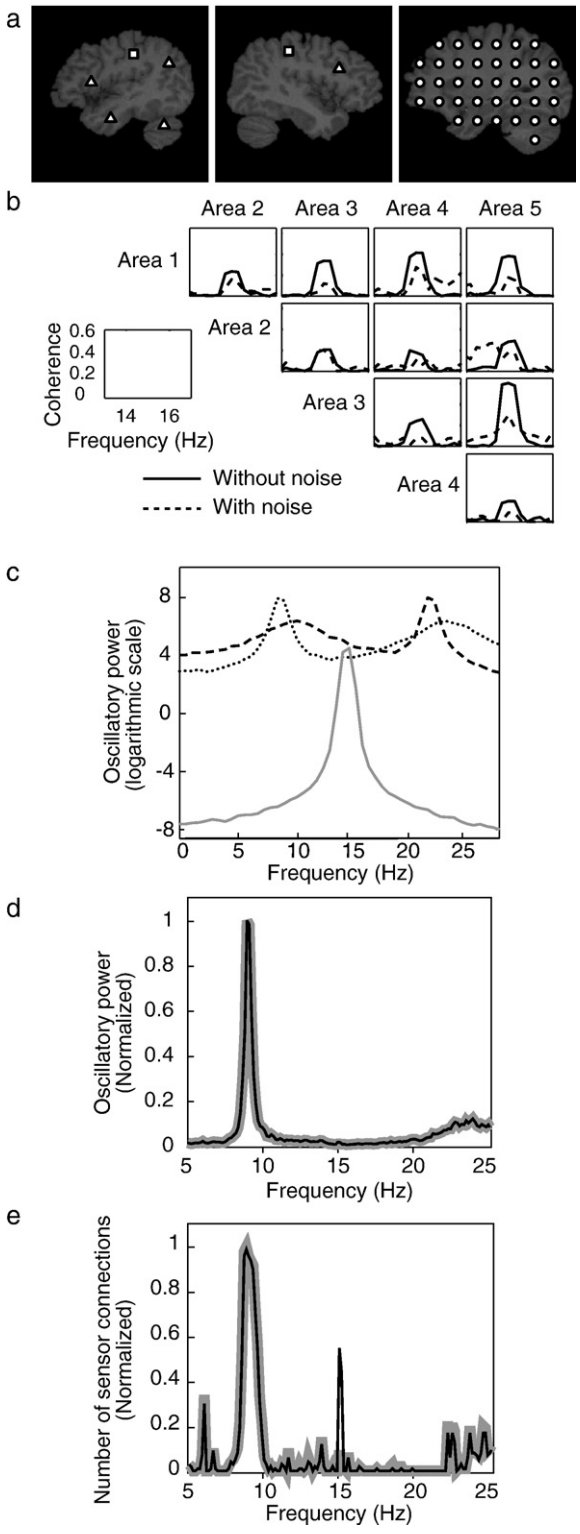

Fig. 1. Simulated data: source locations and sensor-level spectra. (a) Locations of coherent sources (frequency range 14–16 Hz; triangles), noncoherent sources (rectangles), and "noise" sources representing background brain activity (circles). (b) Coherence between the five interacting source areas with and without the added noise component (dashed and solid lines, respectively). (c) Oscillatory power of simulated sources, logarithmic scale. The black dashed and dotted lines indicate the power of the two noncoherent sources, and the solid grey line the power of the coherent sources (peak at ~15 Hz). (d) Oscillatory power and (e) number of coherent connections for one MEG sensor. The thick gray curve represents the *non-coherent* condition, the thin black curve the *coherent* condition.

Simulated data sets were generated separately for 9 subjects (different brain geometries, different positions of the sensor array with respect to the head; subject properties were taken from Kujala et al., 2007). There were three simulation runs, with different amounts of interindividual variation introduced in the source locations (0 mm, i.e., exactly the same locations in all subjects; 5–7 mm, i.e., some variation, approximately matching the grid size used in DICS analysis; 10–12 mm, i.e., larger variation, reflecting extensive anatomical variability of functionally similar areas).

In addition to this *coherent* condition, a *noncoherent* condition was generated in which the coherence between the five interacting sources remained below 0.1 (without the added noise component). The distribution of instantaneous frequencies was similar to the *coherent* condition (base frequency 15 Hz, same amount of random component). The "mask" sources and the noise profile were similar to the *coherent* condition. As illustrated in Fig. 1d, there were no noticeable differences in the power spectra of the two conditions but a marked difference in the connectivity spectra at ~15 Hz (Fig. 1e). In addition, the most powerful oscillations in the data (at ~9 Hz) were evident in the connectivity spectra (spurious coupling), but the amount of connectivity at this frequency was identical in the two conditions.

Results

Evaluating the method with simulated data

Finding reference areas

The simplest way to identify potential reference areas is to localize sources of oscillatory power at a given frequency range. Fig. 2a exemplifies the localization of a noncoherent source based on its oscillatory power at 8–10 Hz. For the coherent sources, however, this approach was not rewarding: The spatial distribution of power at 14–16 Hz did not agree with any of the source locations in the simulated data (Fig. 2b). This discrepancy was due to the fact that the correlated sources elicited only weak power traces (SNR < 0.5 for all coherent sources at 14–16 Hz). When the external reference signal was used to find coherently active areas in the brain (Fig. 2c), the location of maximum coherence corresponded accurately to that of a simulated source (difference between actual and computed location <2 mm in every subject).

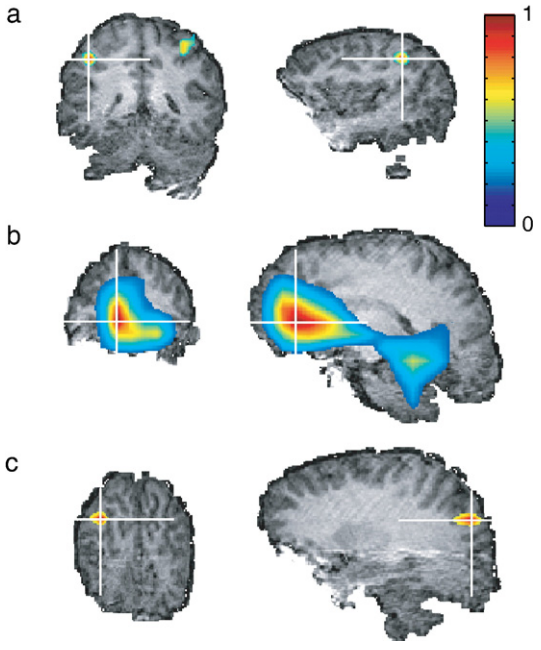

Fig. 2. Localization based on power and external signal-MEG coherence. Localization of (a) maximum power at 8–10 Hz (strongest component at the sensor level), (b) maximum power at 14–16 Hz (coherent frequency band), and (c) strongest external signal-MEG coherence at 14–16 Hz using DICS. The power maps were normalized to the highest power and the coherence map to the strongest coherence in the brain.

The most general approach to obtain reference areas is to identify them directly from cortico-cortical coherence. Fig. 3a shows maxima of the connection density estimate (CDE) in one subject (*coherent* condition). Of the eight identified maxima, five corresponded well to the five simulated source areas (difference 3–7.5 mm, mean 5.5 mm; spurious areas are marked with a black box). There was no systematic bias toward errors in a specific direction. For the 9 subjects, 6–9 focal maxima were identified from the CDE maps. All the coherent areas were localized in each subject, i.e., there was a focal maximum in the CDE map within 1 cm of the original source location. In addition, 1–4 spurious reference areas were localized per subject. Fig. 3b shows the results of contrast connection density estimation (cCDE) between the *coherent* and *noncoherent* conditions. The contrast improved the localization (difference between actual and computed location 1.3–4.6 mm, mean 3.2 mm; cCDE vs. CDE, paired samples *t*-test, $t(4)=3.9$, $p<0.05$) but did not eliminate the spurious findings entirely.

CDE analysis: effect of analysis parameters

Multiple parameters influence the number of correctly and spuriously identified network nodes and the localization accuracy, most notably the grid size and amount of regularization used in DICS computation, and the required minimum distance between connected areas in CDE analysis (Fig. 4). When the grid size was increased from 6 to 12 mm, the number of detected nodes decreased, both in the correct (one-way ANOVA, $F(3)=3.2$, $p<0.05$) and spurious ($F(3)=8.6$, $p<0.01$) category, and the localization errors became larger ($F(3)=3.3$, $p<0.05$). Increasing regularization had essentially the same effect on the detection of network nodes: both the number of correctly ($F(2)=53.5$, $p<0.001$) identified and spurious ($F(2)=153.5$, $p<0.001$) nodes decreased. At the highest regularization level, almost no spurious nodes were detected but, at the same time, only about 30% of the coherent nodes were identified correctly. The value of the required minimum distance between connected areas (4–6 cm) had no significant effect on node detection or localization accuracy.

Sources with a salient, dominant direction of current flow are likely to represent an accurate localization of a focal functional area. Limiting the coherence estimates to sources with relatively fixed orientations of current flow could thus improve detection of correct nodes while reducing detection of spurious sources. Fig. 5 implies that this is the case for simulated data. The dominant orientation of sources was calculated based on singular values of cross spectral estimates at source level. In this simulation (one subject), a ratio of 3 between the two singular values was sufficient to enhance detection of correct nodes and reduce the number of spurious nodes. When the ratio was not limited at all, the number of spurious areas, in particular, was markedly increased.

Fig. 6 compares identification of reference areas from individual vs. group-level CDEs. Whether group-level analysis

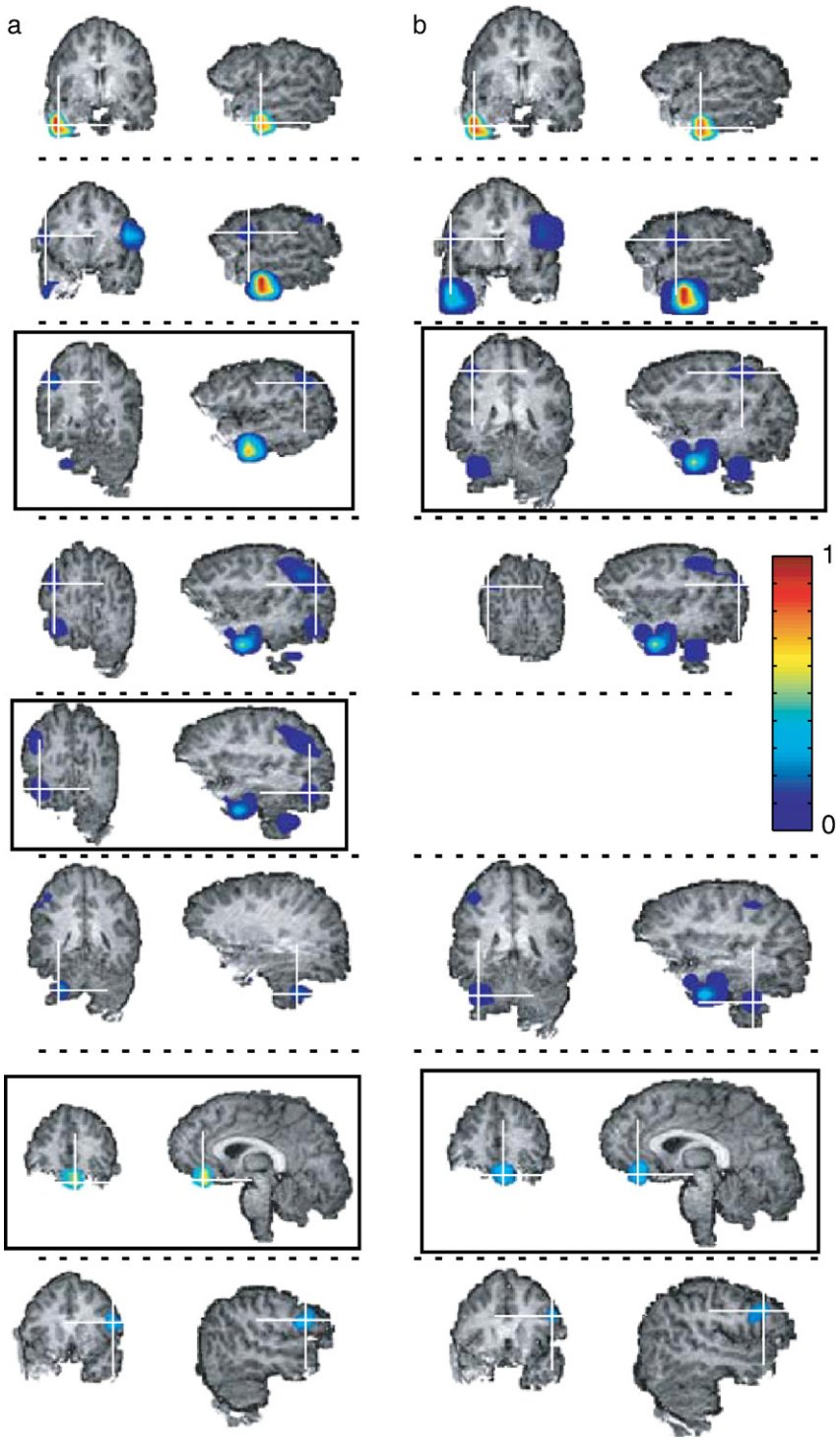

Fig. 3. Connection density maxima for a single subject. (a) Focal maxima of connection density estimate maps (CDEs) at 14–16 Hz for the *coherent* condition. Each point in these maps gives the number of connections from that voxel to all other voxels in the brain, normalized to the highest number of connections per voxel in this subject. (b) cCDE maxima for *coherent* vs. *noncoherent* condition. The cCDE maxima represent areas which were more densely connected to other areas in the *coherent* condition than in the *noncoherent* condition. The slices for both CDE and cCDE maps advance from lateral (top) to medial (bottom) areas, with the single right-hemisphere maximum at the bottom. Here, a minimum distance of 4.5 cm between voxels was used, and areas for which coherence exceeded 0.1 were defined as coupled. Furthermore, the coherence estimation was limited to areas which had a relatively fixed source orientation (cf. Methods and Fig. 5). Corresponding areas identified using CDE and cCDE are shown on the same row. Spurious findings are marked with a black box.

enhances or reduces the sensitivity and accuracy of the estimates depends on the amount of interindividual variability in the locations of the network nodes. Here, CDE was performed on data sets in which the interindividual variation assumed three different values. The CDE maps were computed separately for all subjects using grid size of 6 mm, relative regularization of 0.001,

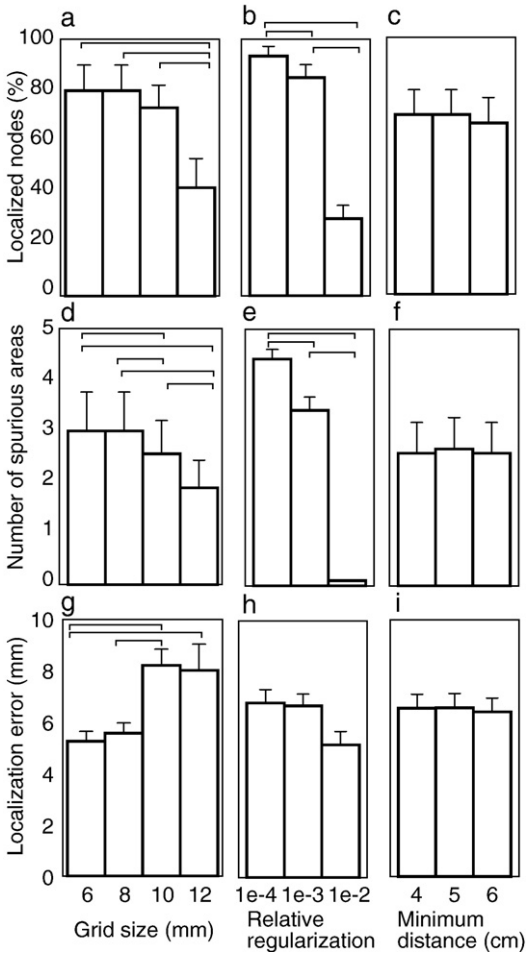

Fig. 4. Effects of parameter choices on CDE. Percentage of identified real sources, number of identified spurious sources, and localization accuracy in CDEs (rows from top to bottom; mean+SEM) as a function of grid size, amount of regularization, and minimum distance between sources (columns from left to right). Regularization is expressed as relative regularization (see Methods). Significant differences (paired samples *t*-test, $p<0.05$) are marked with brackets.

minimum distance of 5 cm and singular-value ratio of 5. Individual reference areas were selected by identifying focal maxima from the CDE maps separately for each subject. Group-level CDE was obtained by combining the individual CDE maps (after a spatial normalization), and focal maxima were identified from this group map. The mean localization error for the five nodal points determined from the individual CDEs was compared with estimation of those same nodes from the group-level maps (transferred to individual anatomy). There was a significant interaction between intersubject variability and individual/group-level analysis (repeated-measures ANOVA, $F(1,16)=11.1$, $p<0.01$). Fig. 6 shows that group-level analysis, indeed, improved localization accuracy when there was no interindividual variability in the simulated source locations ($t(8)=3.8$, $p<0.01$). Introduction of variability, 5–7 mm or 10–12 mm, reduced the effectiveness of the group-level analysis, rendering analysis at the individual level more accurate ($t(8)=2.9$ for 5–7 mm, $p<0.05$; $t(8)=4.5$, $p<0.01$ for 10–12 mm). For intersubject variability of 10–12 mm, localization from group-level maps was, on average, 4 mm less accurate than when the nodes were identified separately from the

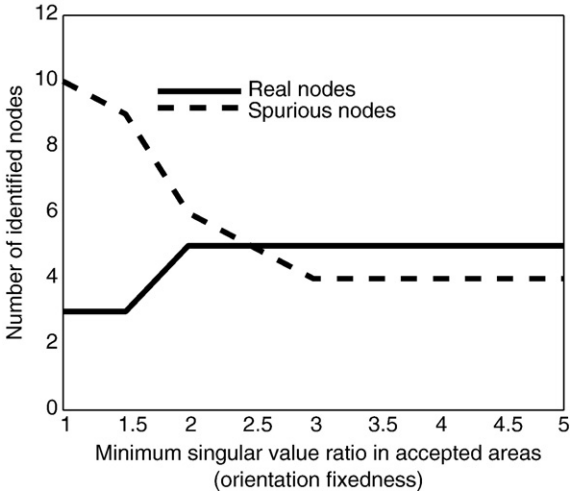

Fig. 5. Effect of source orientation fixedness on CDE. Number of identified real (solid curve) and spurious (dashed curve) network nodes as a function of the singular value ratio (estimate of source orientation fixedness) in one subject.

individual maps. For the group-level analysis, increase in variability systematically increased the localization error (one-way ANOVA, $F(2)=21.4$, $p<0.001$). For individual level analysis, the localization error remained essentially the same (one-way ANOVA, $F(2)=0.2$, $p=0.8$, n.s.). Mislocalization of a reference area may have an adverse effect on further network analysis. A localization error of 10 mm can reduce the estimated level of coherence with other nodes to 50% of the actual value, and to 80% even for a relatively minor mislocalization by 5 mm. Such a drop may suffice to reduce the coherence estimate below the confidence level.

Cortico-cortical mapping at individual and group level

When a spatially and functionally comparable reference area can be identified systematically across individuals, it is possible to search for cortico-cortical connections directly at the group level by computing coherence maps starting from the common reference area and testing the maps for significant group-level effects (e.g.,

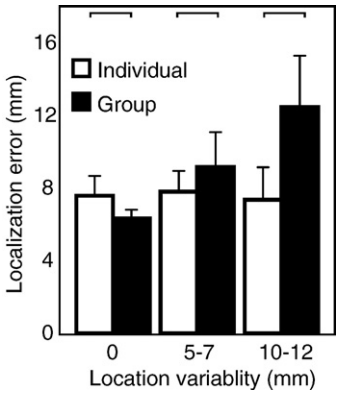

Fig. 6. Accuracy of group-level CDE. Error in localizing the nodal points (mean+SEM) from individual vs. group-level CDE when the intersubject variability was increased from 0 mm through 5–7 mm to 10–12 mm in three simulations. Significant differences (paired samples t-test, $p<0.05$) are marked with brackets.

one-sample *t*-test in SPM2). Fig. 7a shows the results of such an analysis performed on the simulated data. Here, the common reference area was localized using the external reference signal. All the remaining four coherent sources (cf. Fig. 1a) were evident in the group-level map (difference between the actual and observed source locations 3.3–5.1 mm, mean 3.8 mm). In addition, two spurious areas survived to the group level.

In the more general approach, cortico-cortical mapping was performed separately for each individual. The focal CDE maxima (cf. Fig. 3a) were taken as reference areas for computing coherence maps in the entire brain. Fig. 7b depicts the reference areas and the identified additional nodes in one subject. The correctly identified five reference areas led to a total of six real and two spurious nodes. Three of the CDE maxima were spurious findings (black boxes), and only one of them suggested a further connection elsewhere in the brain, to one of the noncoherent sources. As some connections may obviously lead back to other reference areas, one always needs to assess the uniqueness of the identified nodes. Fig. 7 indicates that, e.g., the first reference area and the first connection from the third reference area are within millimeters from each other and are, therefore, likely to represent the same node. DICS can typically distinguish between two source areas as separate if they are located at a distance of 2–3 cm from each other; the more orthogonal the directions of current flow in the two areas are, the smaller the distance required for separation is (Liljeström et al., 2005). When multiple sources fell within 2–3 cm of each other, their mean location was used to represent the area. Of the 15 candidate nodes observed in this subject, 7 separate areas were eventually identified.

After the candidate network nodes had been determined in the individual subjects, surrogate data were used for estimating the 99% confidence level of coherence for all connections in order to limit the final set of nodal points to significantly coupled areas. Fig. 8 shows significance estimation of coherence between the 7 areas identified for the subject presented in Fig. 7. Areas 1–5 (Fig. 8a) correspond to the five coherent source areas (within 7.0± 1.6 mm of the original source location), area 6 to one of the noncoherent source areas with strongest power at 14–16 Hz (cf. Fig. 1), and area 7 to a source area midway between two of the coherent nodal points. For this subject, five connections passed the statistical test (1–2, 1–5, 2–3, 2–5, 3–4) (Fig. 8b). Accordingly, all the five coherent areas and only those areas were accepted into group analysis. Across subjects, 6–10 areas were originally included in the candidate networks. Out of them, 4–7 areas passed the confidence threshold and were included in the further group-level testing. Across simulations, for all subjects, at least four correctly identified areas passed the confidence level estimation (in total 98% of the real nodes survived the testing). Maximally three subjects had up to two spurious connections which passed the confidence level estimation (2.4% of all spurious connections).

Network identification: from the individual to group level

One may wish to focus further characterization of the network (e.g., phase synchronization, direction of information flow) solely on the nodes that were found systematically across subjects. We estimated the between-subjects consistency of network nodes when the five coherent sources across subjects were located in exactly matching anatomical sites, and when an interindividual variation of 5–7 mm or 10–12 mm was introduced in the simulated source locations. When the individually determined nodes were given an extent of 6 mm (one grid space) in each direction and the variation was 0 mm or 5–7 mm, all five simulated nodes were evident in the group maps (in at least 4 subjects). At interindividual variability of 10–12 mm, the extent of one grid spacing revealed only four simulated nodes. However, when the extent was increased to 9 mm (1.5 times the grid spacing), all five nodal points were again consistently detected across subjects. When the extent was increased further to 12 mm (twice the grid spacing), two spurious areas emerged in the group data, in addition to the five simulated nodes.

An important practical question is whether it is sufficient and reasonable to adopt the group-level network nodes or whether it would be beneficial to adjust the exact location of the nodal points according to the individually determined nodes. Exact localization of the reference area has a strong effect on the estimated coherence values. Fig. 9a compares the mean localization error of the five coherent areas, across subjects, when the nodes were determined from the group-level consistency maps (transferred back to the individual coordinate systems) and from the individual coherence maps. Repeated-measures ANOVA showed a significant interaction between the intersubject variability and individual/group-level analysis in the localization accuracy ($F(1,16)=5.6$, $p<0.05$). When there was no variation between subjects, the group-level analysis was more accurate ($t(8)=5.0$, $p<0.01$). When the variation was 10–12 mm, the individual level analysis was more accurate ($t(8)=5.6$, $p<0.01$).

An alternative approach is to use individual nodal points to refine the network identified at the group level. The final network can be obtained by replacing a group-level nodal point with the individual nodal point if one can be found within a predefined distance from the group-level locus. Fig. 9b demonstrates how the localization is affected when the required minimum distance for replacing a group-level node by the corresponding individual node is varied between 5 and 20 mm in 5-mm steps, or when using group-level loci only (i.e., required minimum distance 0 mm). The interaction between the distance criteria and intersubject variability reached significance (repeated measures ANOVA, $F(4,40)=3.4$, $p<0.05$). When there was no intersubject variability, and when the intersubject variability was 10–12 mm, the differences in the localization accuracy were significant (no variation, $F(4)=8.5$, $p<0.001$; 10–12 mm variation, $F(4)=16.1$, $p<0.001$). When the source locations were exactly the same in all individuals, the group-level localization and localization using the 5-mm distance criterion were more accurate than the localization using the larger distance criteria ($t(8)>3.0$, $p<0.05$), with no difference between the distance criteria exceeding 10 mm. When the intersubject variation was 5–7 mm, all selection approaches yielded approximately the same mean error of localization. When the intersubject variation was 10–12 mm, localization was more accurate with all the four different distance criteria than using the group-level nodes ($t(8)>3.1$, $p<0.05$). Furthermore, localization was the more accurate the larger the distance criterion used ($t(8)>2.4$, $p<0.05$). Here, the marked improvement in localization was due to the increase in the number of accepted individual-level nodes (12/45 for 5 mm, 28/45 for 10 mm, 38/45 for 15 mm, and 43/45 for the 20-mm distance criterion).

Application to real data

We evaluated whether the external-reference and CDE approaches yield similar results in localizing cortical reference areas, using a finger movement task. A data set recorded during

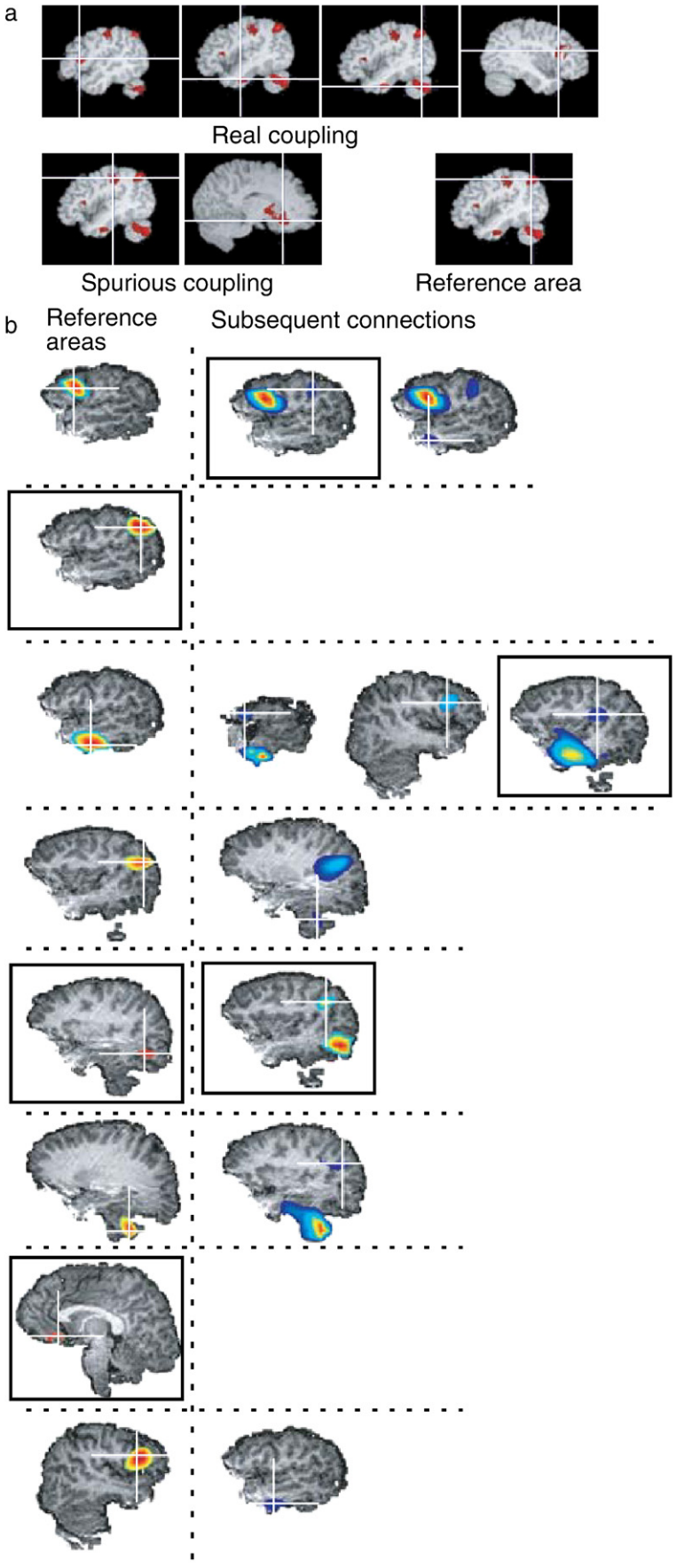
a
Real coupling
Spurious coupling
Reference area
b
Reference areas
Subsequent connections

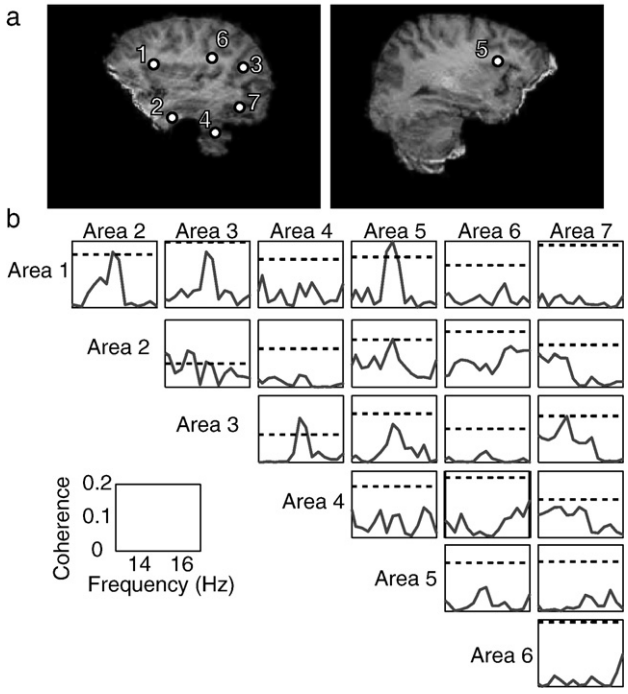

Fig. 8. Significance estimation. (a) Identified areas and (b) coherence between them (one subject). The solid lines represent the estimated coherence between areas and the dashed lines the 99% confidence levels of coherence. Areas 1–5 correspond to the coherent nodes of the network, area 6 corresponds to a noncoherent source area with high power at 14–16 Hz range (spurious connectivity), and area 7 lies between two of the real sources.

reading was employed to investigate whether cortico-cortical networks can be constructed systematically across subjects without an external reference signal.

Finger movements, with an external reference signal

The first data set was collected from 9 healthy, right-handed subjects while they performed continuous, self-paced horizontal flexion and extension movements with their right index finger (Gross et al., 2002). Brain activity was recorded with a whole-head Neuromag 122-channel MEG system, band-pass filtered at 0.03–330 Hz, and sampled at 1 kHz. Surface EMG was measured from the right hand and arm muscles.

EMG–MEG coherence showed a salient maximum at 6–9 Hz that revealed a strong node in the primary motor cortex (M1), in all 9 subjects. When coherent cortico-cortical connections starting from M1 were estimated in the same frequency range, the premotor cortex was identified in all subjects. Fig. 10a shows, for one subject, M1 localized based on EMG–MEG coherence, the subsequently identified premotor cortex, and the group-level result when coherence maps were computed starting from M1 and submitted to one-sample *t*-test in SPM2. Both the common reference area (M1) and the premotor cortex were evident in the group-level statistical map.

Meaningful cortical reference areas were also found directly from the MEG signals by using CDE in the left hemisphere. The estimation produced multiple maxima, but for all 9 subjects two of the maxima corresponded to the M1 and premotor cortex. Here, the orientation fixedness constraint was used to improve the localization. The singular value ratio (estimate of source orientation fixedness) was varied between 1.5 and 3 in order to limit the analysis of coherence to about 10% of all connections in each subject. Fig. 10b shows the CDE maxima corresponding to M1 and premotor cortex for the same subject as in Fig. 10a, and the center points of these two maxima for all 9 subjects. The differences in localizing M1 and the premotor cortex from EMG–MEG coherence or using CDE on MEG data were 7.5±1.2 (mean± SEM) for M1 and 8.1±0.9 for the premotor cortex (values for all individuals in Fig. 10c). The differences were not biased to a specific direction.

Continuous reading, without external reference signal

The second data set was recorded during a paradigm in which words were presented visually in a rapid sequence (Kujala et al., 2007). Nine healthy, native English-speaking subjects participated in this study. Words forming a continuous story were presented in separate blocks at three individually determined rates. At the slowest rate (5–12 words/s), the subjects could understand the story easily, at the medium rate they could comprehend part of it, and at the fastest rate (20–30 words/s) they were unable to follow it. In addition, words were presented in a mixed order at the slowest rate. Brain activity was recorded with an Elekta-Neuromag VectorView MEG system, pass-band filtered at 0.03–200 Hz and digitized at 600 Hz.

There were no meaningful external reference signals available. Hence, CDE was used to localize initial reference areas. The locations of the CDE maxima were too variable for identification of a common reference area for all subjects. Thus, the cortico-cortical networks had to be identified by finding coherent connections from multiple reference areas, separately for each subject (12–18 areas in total). Fig. 11a shows the results of the network identification where connections exceeding the 99% confidence level were included in the intersubject consistency test. The end points of those connections were given an extent of twice the grid spacing, and nodes that had been detected in at least four subjects were accepted as nodal points of the network. Nine distinct regions were identified from the group map. The labels for the nodal points were obtained by transferring the areas of each subject to a template created by the Montreal Neurological Institute (MNI) (Collins et al., 1994) using SPM2. The corresponding Talairach coordinates were determined using a nonlinear transform of MNI to Talairach (Brett et al., 2002). Fig. 11b shows a surface projection of all the individually determined nodes (12–18 per subject). Of the individual-level significantly coupled nodes, 53% were located within 1 cm of a group-level node, as denoted by the

Fig. 7. Cortico-cortical connections. (a) Cortico-cortical connections at the group level, starting from a common reference area. The connections were estimated by calculating the individual coherence maps and submitting them to a one-sample *t*-test in SPM2. In each view, the crosshairs indicate the maximum on which the slice was centered. (b) Coherent connections (coherence>0.1), starting from CDE-based reference areas, in one subject. The left-most column portrays the coherence of a reference area with itself. Spurious reference areas and spurious connections are marked with a black box. In this subject, two of the spurious CDE maxima did not yield focal connections exceeding the threshold (0.1). One spurious reference area (fifth row) yielded a clearly focal connection that exceeded the threshold.

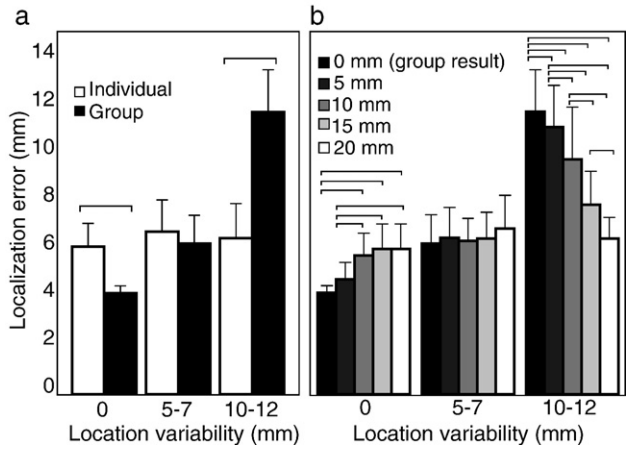

Fig. 9. Accuracy of network identification at group level and individual level. (a) Localization error (mean+SEM) when nodal points were determined from group-level data and when nodal points were determined from individual results, for three levels of interindividual variability in node locations. (b) Localization error (mean+SEM) of nodes determined from group results and individual maps when the distance criterion for replacing a group-level node with an individual nodal point was varied from 0 to 2 cm. Significant differences (paired samples t-test, $p<0.05$) are marked with brackets.

colored dots and spheres. Further characterization of the group-level nodes, based on cortical time-series of activation, produced systematic results across subjects on phase coupling and direction of information flow (Granger, 1980; Tass et al., 1998; Roebroeck et al., 2005) that mirrored the subjects' ability to comprehend the text (Kujala et al., 2007).

Discussion

Hemodynamic and neurophysiological methods have been used to assess cortico-cortical interactions noninvasively, typically by first localizing areas that show task-specific activations. Coupling within the network has then been characterized by either directly calculating interactions between its nodes or in a hypothesis-driven approach, by constructing models of interactions and fitting the measured data to them. A limitation here is that the activated areas, or areas in which activity is modulated by the task, are not necessarily the most relevant nodes of the interacting cortical network. Alternatively, one can identify cortico-cortical networks in a data-driven manner, by first selecting a reference area in the brain, and then locating other areas with time-courses of activation coupled to that in the reference area (Gross et al., 2001; Fox et al., 2005; Fox et al., 2006; Kessler et al., 2006). Here, a possible problem lies in the large number of degrees of freedom, i.e., it may be difficult to identify convergent networks across subjects, especially ones that are highly relevant to the studied task. In electromagnetic methods (EEG, MEG), external reference signals can facilitate identification of cortical reference areas. Recording of hand or arm movements has been particularly powerful in this regard (Gross et al., 2002; Butz et al., 2006; Jerbi et al., 2007). In hemodynamic methods (fMRI), interaction analysis has also been performed by calculating correlations between all voxels or among a large number of predefined areas (Eguiluz et al., 2005; Achard et al., 2006). The same type of approach has been applied to MEG data as well at the sensor level (Bassett et al., 2006; Langheim et al., 2006; Stam et al., 2006). However, regardless of the approach used in the connectivity analysis, it is not possible to evaluate whether the connectivity structure of the identified areas explains the variance of the measured data in the same direct manner as in activation studies. The set of identified areas may form only a portion of the entire network and provide a misleading representation of the connectivity pattern (Salmelin and Kujala, 2006).

Here, in order to gain better understanding of how the choices made at different stages of the analysis affect the outcome, we simulated a realistic MEG experiment, with multiple participants. The simulated data were constructed to resemble real data, i.e., the activity of the interacting nodal areas was too weak to be identified based on their oscillatory power, and the localization had to rely on coupling measures. Furthermore, the anatomical correspondence of the simulated sources between subjects was systematically varied and the effect of such interindividual variability on connectivity estimates evaluated. The DICS analysis approach was further applied to two real data sets to demonstrate its functionality.

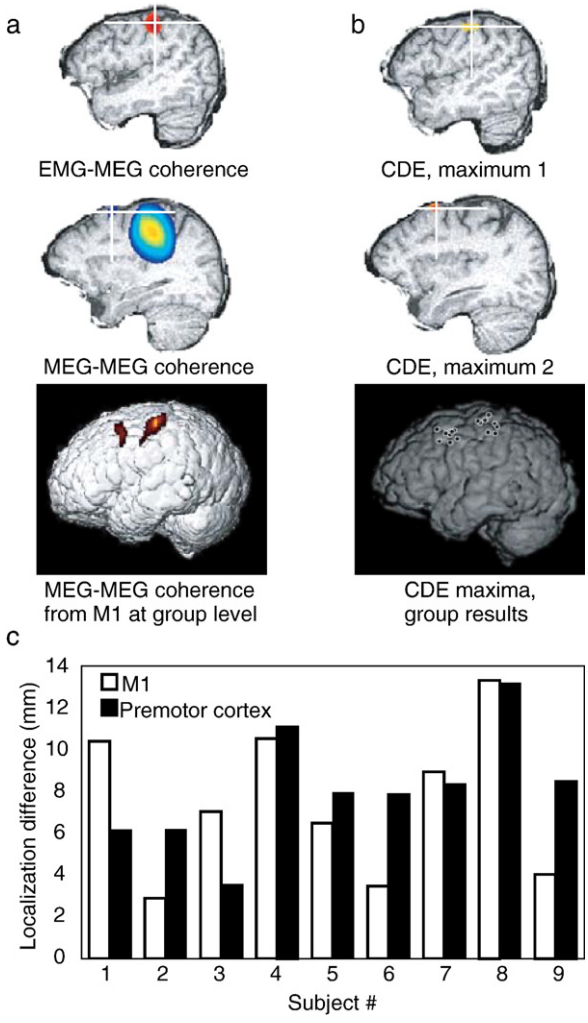

Fig. 10. Slow finger movements: EMG–MEG coherence vs. CDE. Identification of cortical networks for one subject when reference areas were localized using (a) EMG–MEG coherence and (b) CDE. Group-level results are depicted below. (c) Difference between EMG–MEG and CDE localization for nodes in the motor cortex (M1) and premotor cortex in each of the 9 subjects.

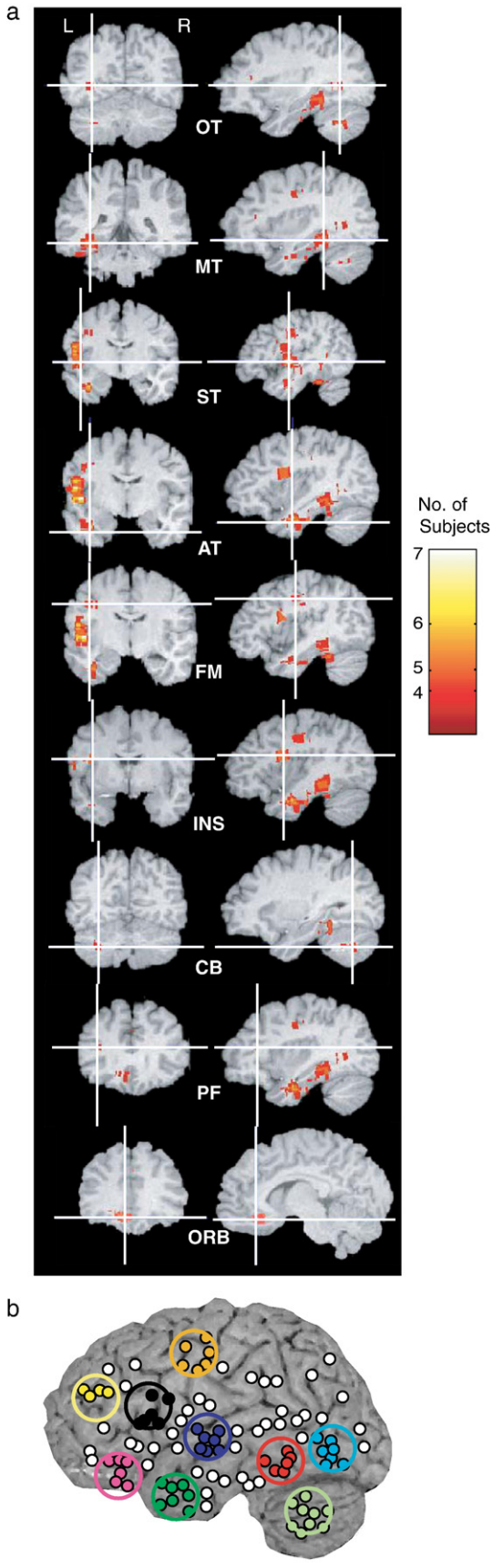

Perhaps the greatest risk in coupling analysis are false positives, i.e., detection of spurious areas that are simply artifacts of the neuroimaging and analysis methods and play no meaningful role in the network. With electromagnetic measures, it is possible that a detected connection results from a single source area that is erroneously regarded as two spatially separate regions with synchronized time-courses of activation. The present DICS analysis is, in principle, susceptible to spurious connectivity starting from the identification of the frequency ranges of interest. Peaks in sensor-sensor coupling at specific frequencies may be due to activity leaking to multiple sensors, which could even pass significance testing. However, it should be possible to identify and reject such spurious features using multiple experimental conditions. Even though perfectly power-matched control conditions cannot usually be created, well-matched ones should enable identification of frequencies at which the amount of coupling, but not the amount of oscillatory power, is affected by the experimental condition. Here, for the simulated data, sensor-level connectivity analysis allowed detection of frequencies at which there was coupling but no evident power. Furthermore, inclusion of a power-matched control condition in which activity was noncoherent made it possible to discern the frequencies relevant for interareal connectivity from those with high power only.

At the cortical level, part of the nodal points emerging in the analysis will most likely be spurious even if they appear to be focal and located in functionally meaningful areas. In the present simulation, use of an external reference signal resulted in very accurate localization of a common cortical reference area across subjects (localization error <2 mm), and the subsequent localization of the network with group-level SPM2 analysis resulted in identification of all the interacting areas. However, in addition to the actual simulated nodes, two spurious areas passed the group-level consistency test. Spurious areas appeared also when the data analysis was performed solely on the basis of MEG signals, using connection density estimation (CDE). By using contrast CDE maps (coherent vs. noncoherent condition), spurious maxima were reduced in number although not completely eliminated. When the reference areas had been identified correctly, the proportion of spurious nodes was relatively small, and this ratio was further improved by estimation of confidence level, based on surrogate data. The surrogate data should be selected carefully, as they must be justified by the data (Schreiber and Schmitz, 2000). Specifically, when choosing the surrogate data in coherence analysis, one should consider whether the signals can be assumed to be independent. For example, coherence between two time-series could be destroyed either by randomizing their time samples similarly or their phases differently. In beamforming, however, this type of phase-randomized surrogate data would not preserve the spatial filter leakage properties. Here, time-randomized surrogate

Fig. 11. Reading: Group-level nodal points of neural connectivity. (a) Section overlays of brain areas in which the time-courses of activation at 8–13 Hz were significantly coherent with those in other regions of the brain. This map indicates intersubject consistency of spatial location of the nodes (color denotes number of subjects). OT = inferior occipitotemporal cortex, MT = medial temporal cortex, ST = superior temporal cortex, AT = anterior part of the inferior temporal cortex, FM = face motor cortex, INS = insula, CB = cerebellum, PF = prefrontal cortex, ORB = orbital cortex. (b) Surface projections of all individual level nodes exceeding 99% confidence level (dots) and their clustering to group-level nodal points (colored dots and circles).

data sets were constructed specifically to test for spurious coherence due to leakage between spatial filters. When the confidence level was set at 99% (based on surrogate data), 98% of the real nodes, and 2.4% of the spurious connections survived the test.

Based on the present simulation of a realistic experimental data set, there is no simple optimal choice of parameters for the analysis. For example, the number of spuriously detected areas could be reduced by increasing either the grid size or the regularization, but at the cost of compromising spatial specificity and finding fewer of the true nodal areas. Varying the required minimum distance between source areas appeared to have no practical effect on the accuracy of localization. This stability was most likely due to the fact that the distances varied from 4 to 6 cm, which are clearly above the spatial resolution of MEG (2–3 cm; Liljeström et al., 2005). Hence, the leakage between spatial filters and, accordingly, detection of spurious coupling was reduced. Thus, our simulations indicate that for real data sets a grid size of ~5 mm, which is still computationally feasible, a moderate level of regularization, and a minimum distance of 4 cm between sources would seem reasonable choices.

The clearest improvement in the localization accuracy was achieved by demanding a fixed orientation of current flow within each voxel for which coherence was estimated. This approach both decreased spurious detection and increased identification of real nodal areas. The demand of relatively fixed orientation is well based in neurophysiology. In order for a neuronal event to be detected with MEG, thousands of pyramidal cells within a small cortical patch need to be activated simultaneously. The parallel orientation of the apical dendrites of these neurons facilitates the summation of the neural currents. Candidate nodes with a salient, dominant direction of current flow are thus more likely to represent accurate localization of a focal functional area than nodes with no preferred orientation. In the simulations, we used point-like sources with perfectly fixed orientations to represent the sources. In real data, the efficiency of the orientation fixedness criterion is influenced by the spatial extent and depth of the sources and the signal-to-noise ratio. Here, when a moderate orientation fixedness constraint was applied on the real data set in which subjects performed finger movements, both M1 and the premotor cortex could be identified from the CDE maps in all subjects, and the nodes were located within ~8 mm of the loci determined from the EMG–MEG coherence.

Another important question in coupling analysis is whether it should be performed at the individual or group level. Our simulations showed that when the interindividual variation in node locations was set to zero, identification of reference areas from the CDE was more accurate at group than individual level. However, as soon as some variability was introduced in the locations (>5 mm), CDE was more accurate at individual than group level. The relative merits of individual vs. group-level analysis were quite similar in identification of the final network as well. When there was no variability in the location of the simulated source areas between subjects, group-level nodes represented the network more accurately than individual-level nodes. In contrast, when the variation was 10–12 mm, localization was more accurate at the individual than group level. It appears that in localization of interacting areas the benefits obtained from increased statistical power are relatively small and that group-level analysis of connectivity, both at the stages of identifying reference areas and final networks, is more accurate than network analysis in individual subjects only when the variation across subjects remains small.

Also, in the group-level identification, the spatial extent given to the sources, the grid size and the interindividual variability of node location played an important role. When the interindividual variation (0, 5–7 mm) and the spatial extent given to the individual nodes (6 mm) both remained approximately within the grid size (6 mm), only the five correct nodes survived the intersubject consistency test. When the interindividual variation was increased to 10–12 mm, only four of the real areas were detected in the group map. When the spatial extent given to the nodes was increased to the same level as the variation in location (12 mm), all five nodal points again passed the test, but spurious areas additionally emerged. Thus, an estimate of the magnitude of interindividual variability would clearly help to ensure that the correct nodes would be identified.

Here, coherence was used to image interaction between cortical areas. Thus, this analysis would not detect connectivity between cortical regions if the amplitudes of the coupled areas were entirely random or if their coupling was nonlinear or reflected solely as phase locking. Phase locking (Lachaux et al., 1999; Rodriguez et al., 1999; Simoes et al., 2003) and phase synchronization (Tass et al., 1998; Rodriguez et al., 1999; Gross et al., 2004; Palva et al., 2005) would be better suited for imaging those types of interactions. These measures, however, require an accurate estimation of source orientation and the extraction of time-series in each cortical location of interest. In practical use, measures of signal phase are typically evaluated for brain areas that have been first identified by computationally more efficient approaches, such as localization of power or coherence (Gross et al., 2001; Gross et al., 2002; Gross et al., 2004; Kessler et al., 2006). Neural interactions can also be imaged by evaluating effective connectivity between cortical areas, e.g., with Granger causality. Naturally, if there is no information flow directly between areas or if the apparent information flow is caused by interaction due to common input, causal measures would not describe the coupling correctly. Thus, it may be prudent to use multiple connectivity measures to evaluate the significance of the findings. For example, converging group-level results from both phase synchronization and causality analysis would be strong evidence that the identified connections reflect true connectivity and are not, for example, due to leakage of activity from the same source. Combined use of these methods was demonstrated on the data set that was recorded during rapid serial visual presentation of words (Fig. 11; Kujala et al., 2007). The network nodes were identified based on the MEG signals alone, and the analysis produced comparable sets of significantly coherent areas across subjects. Furthermore, both phase synchronization and Granger causality yielded systematic results across subjects between the different experimental conditions, increasing the trust that the identified network indeed played a role in reading.

Direct localization of coupling enables the identification of interacting cortical areas, irrespective of their level of activity, without modeling assumptions such as those required, e.g., in Dynamic Causal Modeling (Friston et al., 2003). The data-driven localization also requires assumptions, such as models for the neural currents and brain geometry and conductivity, but the connected areas and the nature of their mutual interactions are determined directly from the recorded data without *a priori* assumptions. Here, we have shown that by selecting appropriate parameter values it is possible to perform such identification accurately, without excessive spurious connections. For real data, it

is impossible to set all the parameters perfectly, but the present simulations, and examples of real data, should help to better understand how the choices made affect the outcome of the analysis. The considerations on individual vs. group-level analysis, in particular, are likely to be relevant for both electromagnetic and hemodynamic neuroimaging approaches.

Acknowledgments

We are grateful to Mika Seppä for help with coordinate transformations, and to Mia Liljeström and Alard Roebroeck for their comments on the manuscript. This work was supported by the Finnish Ministry of Education, the James S. McDonnell Foundation 21st Century Research Award, the Academy of Finland (Centre of Excellence Programmes 2000–2005 and 2006–2011 and grant no. 115844), and the Sigrid Jusélius Foundation.

References

Achard, S., Salvador, R., Whitcher, B., Suckling, J., Bullmore, E., 2006. A resilient, low-frequency, small-world human brain functional network with highly connected association cortical hubs. J. Neurosci. 26, 63–72.

Ahonen, A.I., Hämäläinen, M.S., Ilmoniemi, R.J., Kajola, M.J., Knuutila, J.E., Simola, J.T., Vilkman, V.A., 1993. Sampling theory for neuromagnetic detector arrays. IEEE Trans. Biomed. Eng. 40, 859–869.

Andres, F.G., Mima, T., Schulman, A.E., Dichgans, J., Hallett, M., Gerloff, C., 1999. Functional coupling of human cortical sensorimotor areas during bimanual skill acquisition. Brain 122, 855–870.

Astolfi, L., Cincotti, F., Babiloni, C., Carducci, F., Basilisco, A., Rossini, P.M., Salinari, S., Mattia, D., Cerutti, S., Dayan, D.B., Ding, L., Ni, Y., He, B., Babiloni, F., 2005. Estimation of the cortical connectivity by high-resolution EEG and structural equation modeling: simulations and application to finger tapping data. IEEE Trans. Biomed. Eng. 52, 757–768.

Bassett, D.S., Meyer-Lindenberg, A., Achard, S., Duke, T., Bullmore, E., 2006. Adaptive reconfiguration of fractal small-world human brain functional networks. Proc. Natl. Acad. Sci. U. S. A. 103, 19518–19523.

Brett, M., Johnsrude, I.S., Owen, A.M., 2002. The problem of functional localization in the human brain. Nat. Rev., Neurosci. 3, 243–249.

Büchel, C., Friston, K.J., 1997. Modulation of connectivity in visual pathways by attention: cortical interactions evaluated with structural equation modelling and fMRI. Cereb. Cortex 7, 768–778.

Büchel, C., Friston, K.J., 1998. Dynamic changes in effective connectivity characterized by variable parameter regression and Kalman filtering. Hum. Brain Mapp. 6, 403–408.

Butz, M., Timmermann, L., Gross, J., Pollok, B., Dirks, M., Hefter, H., Schnitzler, A., 2006. Oscillatory coupling in writing and writer's cramp. J. Physiol. (Paris) 99, 14–20.

Collins, D.L., Neelin, P., Peters, T.M., Evans, AC., 1994. Automatic 3D intersubject registration of MR volumetric data in standardized Talairach space. J. Comput. Assist. Tomogr. 18, 192–205.

Cosmelli, D., David, O., Lachaux, J.P., Martinerie, J., Garnero, L., Renault, B., Varela, F., 2004. Waves of consciousness: ongoing cortical patterns during binocular rivalry. NeuroImage 23, 128–140.

Dale, A.M., Liu, A.K., Fischl, B.R., Buckner, R.L., Belliveau, J.W., Lewine, J.D., Halgren, E., 2000. Dynamic statistical parametric mapping: combining fMRI and MEG for high-resolution imaging of cortical activity. Neuron 26, 55–67.

Eguiluz, V.M., Chialvo, D.R., Cecchi, G.A., Baliki, M., Apkarian, AV., 2005. Scale-free brain functional networks. Phys. Rev. Lett. 94, 018102.

Faes, L., Pinna, G.D., Porta, A., Maestri, R., Nollo, G., 2004. Surrogate data analysis for assessing the significance of the coherence function. IEEE Trans. Biomed. Eng. 51, 1156–1166.

Fox, M.D., Snyder, A.Z., Vincent, J.L., Corbetta, M., Van Essen, D.C., Raichle, M.E., 2005. The human brain is intrinsically organized into dynamic, anticorrelated functional networks. Proc. Natl. Acad. Sci. U. S. A. 102, 9673–9678.

Fox, M.D., Corbetta, M., Snyder, A.Z., Vincent, J.L., Raichle, ME., 2006. Spontaneous neuronal activity distinguishes human dorsal and ventral attention systems. Proc. Natl. Acad. Sci. U. S. A. 103, 10046–10051.

Friston, K.J., Harrison, L., Penny, W., 2003. Dynamic causal modelling. NeuroImage 19, 1273–1302.

Gerloff, C., Richard, J., Hadley, J., Schulman, A.E., Honda, M., Hallett, M., 1998. Functional coupling and regional activation of human cortical motor areas during simple, internally paced and externally paced finger movements. Brain 121, 1513–1531.

Granger, C.W.J., 1980. Testing for causality: a personal viewpoint. J. Econ. Dyn. Control 2, 329–352.

Gross, J., Ioannides, A.A., 1999. Linear transformations of data space in MEG. Phys. Med. Biol. 44, 2081–2097.

Gross, J., Kujala, J., Hämäläinen, M., Timmermann, L., Schnitzler, A., Salmelin, R., 2001. Dynamic imaging of coherent sources: studying neural interactions in the human brain. Proc. Natl. Acad. Sci. U. S. A. 98, 694–699.

Gross, J., Timmermann, J., Kujala, J., Dirks, M., Schmitz, F., Salmelin, R., Schnitzler, A., 2002. The neural basis of intermittent motor control in humans. Proc. Natl. Acad. Sci. U. S. A. 99, 2299–2302.

Gross, J., Schmitz, F., Schnitzler, I., Kessler, K., Shapiro, K., Hommel, B., Schnitzler, A., 2004. Modulation of long-range neural synchrony reflects temporal limitations of visual attention in humans. Proc. Natl. Acad. Sci. U. S. A. 101, 13050–13055.

Halliday, D.M., Rosenberg, J.R., Amjad, A.M., Breeze, P., Conway, B.A., Farmer, SF., 1995. A framework for the analysis of mixed time series/point process data-theory and application to the study of physiological tremor, single motor unit discharges and electromyograms. Prog. Biophys. Mol. Biol. 64, 237–278.

Hillebrand, A., Singh, K.D., Holliday, I.E., Furlong, P.L., Barnes, G.R., 2005. A new approach to neuroimaging with magnetoencephalography. Hum. Brain Mapp. 25, 199–211.

Hämäläinen, M., Hari, R., Ilmoniemi, R.J., Knuutila, J., Lounasmaa, O.V., 1993. Magnetoencephalography—theory, instrumentation, and applications to noninvasive studies of the working human brain. Rev. Mod. Phys. 65, 413–497.

Jerbi, K., Lachaux, J.P., N'Diaye, K., Pantazis, D., Leahy, R.M., Garnero, L., Baillet, S., 2007. Coherent neural representation of hand speed in humans revealed by MEG imaging. Proc. Natl. Acad. Sci. U. S. A. 104, 7676–7681.

Kessler, K., Biermann-Ruben, K., Jonas, M., Siebner, H.R., Baumer, T., Munchau, A., Schnitzler, A., 2006. Investigating the human mirror neuron system by means of cortical synchronization during the imitation of biological movements. NeuroImage 33, 227–238.

Kujala, J., Pammer, K., Cornelissen, P., Roebroeck, A., Formisano, E., Salmelin, R., 2007. Phase coupling in a cerebro-cerebellar network at 8–13 Hz during reading. Cereb. Cortex 17, 1476–1485.

Lachaux, J.P., Rodriguez, E., Martinerie, J., Varela, F.J., 1999. Measuring phase synchrony in brain signals. Hum. Brain Mapp. 8, 194–208.

Langheim, F.J., Leuthold, A.C., Georgopoulos, A.P., 2006. Synchronous dynamic brain networks revealed by magnetoencephalography. Proc. Natl. Acad. Sci. U. S. A. 103, 455–459.

Liljeström, M., Kujala, J., Jensen, O., Salmelin, R., 2005. Neuromagnetic localization of rhythmic activity in the human brain: a comparison of three methods. NeuroImage 25, 734–745.

Mechelli, A., Penny, W.D., Price, C.J., Gitelman, D.R., Friston, KJ., 2002. Effective connectivity and intersubject variability: using a multisubject network to test differences and commonalities. NeuroImage 17, 1459–1469.

Mechelli, A., Crinion, J.T., Long, S., Friston, K.J., Lambon Ralph, M.A., Patterson, K., McClelland, J.L., Price, CJ., 2005. Dissociating reading

processes on the basis of neuronal interactions. J. Cogn. Neurosci. 17, 1753–1765.
Palva, J.M., Palva, S., Kaila, K., 2005. Phase synchrony among neuronal oscillations in the human cortex. J. Neurosci. 25, 3962–3972.
Patel, R.S., Van De Ville, D., Dubois Bowman, F., 2006. Determining significant connectivity by 4D spatiotemporal wavelet packet resampling of functional neuroimaging data. NeuroImage 31, 1142–1155.
Penny, W.D., Stephan, K.E., Mechelli, A., Friston, KJ., 2004. Modelling functional integration: a comparison of structural equation and dynamic causal models. NeuroImage 23 (Suppl. 1), S264–S274.
Priestley, M., 1981. Spectral Analysis and Time Series. Academic Press, New York.
Robinson, S.E., Vrba, J., 1997. Functional neuroimaging by Synthetic Aperture Magnetometry (SAM). In: Yoshimoto, T., Kotani, M., Kuriki, S., Karibe, H., Nakasato, B. (Eds.), Recent Advances in Biomagnetism. Sendai. Tohoku Univ. Press, Sendai, pp. 302–305.
Rodriguez, E., George, N., Lachaux, J.P., Martinerie, J., Renault, B., Varela, FJ., 1999. Perception's shadow: long-distance synchronization of human brain activity. Nature 397, 430–433.
Roebroeck, A., Formisano, E., Goebel, R., 2005. Mapping directed influence over the brain using Granger causality and fMRI. NeuroImage 25, 230–242.
Salmelin, R., Kujala, J., 2006. Neural representation of language: activation versus long-range connectivity. Trends Cogn. Sci. 10, 519–525.
Sarnthein, J., Petsche, H., Rappelsberger, P., Shaw, G.L., von Stein, A., 1998. Synchronization between prefrontal and posterior association cortex during human working memory. Proc. Natl. Acad. Sci. U. S. A. 95, 7092–7096.
Schnitzler, A., Gross, J., 2005. Normal and pathological oscillatory communication in the brain. Nat. Rev., Neurosci. 6, 285–296.
Schormann, T., Zilles, K., 1998. Three-dimensional linear and nonlinear transformations: an integration of light microscopical and MRI data. Hum. Brain Mapp. 6, 339–347.
Schreiber, T., Schmitz, A., 2000. Surrogate time series. Physica, D 142, 346–382.
Sekihara, K., Scholz, B., 1996. Generalized Wiener estimation of three-dimensional current distribution from biomagnetic measurements. IEEE Trans. Biomed. Eng. 43, 281–291.
Simoes, C., Jensen, O., Parkkonen, L., Hari, R., 2003. Phase locking between human primary and secondary somatosensory cortices. Proc. Natl. Acad. Sci. U. S. A. 100, 2691–2694.
Singer, W., 1999. Neuronal synchrony: a versatile code for the definition of relations? Neuron 24, 49–65 (111-25).
Stam, C.J., Jones, B.F., Manshanden, I., van Cappellen van Walsum, A.M., Montez, T., Verbunt, J.P., de Munck, J.C., van Dijk, B.W., Berendse, H.W., Scheltens, P., 2006. Magnetoencephalographic evaluation of resting-state functional connectivity in Alzheimer's disease. NeuroImage 32, 1335–1344.
Tallon-Baudry, C., Bertrand, O., Fischer, C., 2001. Oscillatory synchrony between human extrastriate areas during visual short-term memory maintenance. J. Neurosci. 21, RC177.
Tass, P., Rosenblum, M., Weule, J., Kurths, J., Pikovsky, A., Volkmann, J., Schnitzler, A., Freund, H.-J., 1998. Detection of n:m phase locking from noisy data: application to magnetoencephalography. Phys. Rev. Lett. 81, 3291–3294.
Van Veen, B.D., van Drongelen, W., Yuchtman, M., Suzuki, A., 1997. Localization of brain electrical activity via linearly constrained minimum variance spatial filtering. IEEE Trans. Biomed. Eng. 44, 867–880.
von Stein, A., Rappelsberger, P., Sarnthein, J., Petsche, H., 1999. Synchronization between temporal and parietal cortex during multimodal object processing in man. Cereb. Cortex 9, 137–150.
Xiong, J., Rao, S., Jerabek, P., Zamarripa, F., Woldorff, M., Lancaster, J., Fox, P.T., 2000. Intersubject variability in cortical activations during a complex language task. NeuroImage 12, 326–339.